Supporting Information

Stanika et al. 10.1073/pnas.0903546106

SI Materials and Methods

Cell Culture, Stimulation Protocols, and Survival Assays. Dissociated hippocampal neurons prepared from day 20 embryonic Sprague-Dawley rats were plated onto a glial feeder layer and maintained in growth media for 14–28 days in vitro (DIV). For experiments, cultures of appropriate age were transferred into Hepes-buffered saline solution (HBSS) containing (in mM): 137 NaCl, 10 Hepes, 2.0 $CaCl_2$, 1.0 $MgSO_4$, 5.4 KCl, 0.3 Na_2HPO_4, 0.22 KH_2PO_4, 10 glucose, and 26 sucrose (320 mOsM [pH 7.4]) supplemented with 10 μM glycine. After excitotoxic exposure, cultures were washed in HBSS and returned to the incubator in growth medium for 20–24 h. When appropriate, inhibitors were added to the HBSS 10 min before glutamate or NMDA. Cell death was assayed by propidium iodide (3.3 μg/mL) staining. Immunostaining for NeuN, a neuron-specific protein, was used to assay the total number of neurons. Cell counting was carried out using ImageJ software (freely available at http://rsb.info.nih.gov/ij/index.html).

To achieve selective synaptic activation, we applied either of the GABAergic antagonists bicuculline or picrotoxin. The former was supplemented with 4-aminopyridine and the latter with strychnine and supramaximal concentrations of glycine (300 μM) to enhance the response. In general, cells responded similarly to both agonists. Experiments with fura-2 used PTX instead of bicuculline to avoid photodamage. Control experiments (not shown) addressed 2 potential pitfalls of these protocols: (1) the MK-801 block of synaptic receptors was not significantly reversed for at least 15 min after MK-801 washout; (2) "synaptic" Ca^{2+} transients were similar in the presence and absence of the glutamate transporter inhibitor TBOA. Because TBOA would be expected to enhance Ca^{2+} elevations if there were a significant extrasynaptic component arising from glutamate spillover, this indicates that the synaptic origin of these transients was not contaminated by spillover.

Fluorescence Microscopy. For dye loading, cultures were incubated in 4 μM fura-2 AM or fura-2FF AM in HBSS for 30 min at 37 °C and subsequently imaged using a Zeiss Axiovert 200 light microscope (Carl Zeiss; 40× objective). Images were recorded by means of a CoolSNAP HQ2 CCD camera (Photometrics) controlled by EasyRatioPro software (Photon Technology International). All experiments were performed at 25 °C. For quantitative imaging, fura-based fluorophores were excited alternately at 340 and 380 nm, and fluorescence emission was collected at 510 nm. Free Ca^{2+} concentrations were estimated from the ratio of 340/380 fluorescence intensities using the method of Grynkiewicz et al. (1). Due to the uncertainties inherent in calibration procedures, presented concentrations should be considered estimates. For long-term imaging, cultures were continuously perfused with HBSS containing added drugs as needed. Images were collected at 10- to 30-sec intervals during the initial part of the experiment and at 60- to 120-sec intervals during the remainder.

For MMP assays, cells were loaded for 30 min at 37 °C with low concentrations of tetramethylrhodamine methyl ester (TMRM, 5 nM; Invitrogen) in HBSS; the dye was present in the incubation medium during imaging. Cells were imaged on the Zeiss 510 confocal microscope (40×, 1.3 NA objective, excitation 561 nm, emission >575 nm). For plasma membrane potential assays, cells were loaded with PMPI, a proprietary component of the Membrane Potential Assay Kit R-8042 (Molecular Devices), by incubation with 0.5 μL/mL of PMPI stock for 45 min at 37 °C; the dye (at 0.05 μL/mL) was present during imaging. PMPI fluorescence emission was recorded at 530–600 nm with 514 nm excitation. The computational model of Nicholls (2), with mitochondrial volume fraction estimated as 5% for hippocampal neurons, was used to correct for the contribution of plasma membrane depolarization to TMRM fluorescence loss. Fluorescence was quantified using ImageJ software.

Western Blot Analysis. Frozen lysates of hippocampal cultures were thawed and dissociated on ice using a probe sonicator (2 bursts of 20 sec each at the lowest power setting [<5 W]). Approximately equal amounts of total protein, determined using the bicinchoninic acid protein assay (Pierce), were electrophoresed and subsequently transferred to polyvinylidene difluoride membranes (Invitrogen). Blots were incubated overnight at 4 °C with antibodies to NR2A (559889; BD Pharmingen), NR2B (32–0700; Zymed), NR1 (MAB363; Chemicon), or actin (MAB1501R; Chemicon) at 1:1,000, 1:1,000, 1:2,000, and 1:4,000, respectively. Proteins were detected by chemiluminescence (WesternBreeze; Invitrogen). After development of the blot in one antibody, it was stripped (Restore PLUS Western Blot Stripping Buffer; Thermo Scientific) and reprobed with a different antibody.

Electron Microscopy and Electron Probe X-ray Microanalysis (EPMA). Specimens for structural electron microscopy were generally prepared by high-pressure freezing/freeze-substitution to preserve the Ca-containing mitochondrial precipitates that otherwise leach out during processing, and to avoid any potential swelling artifacts that might accompany slow chemical fixation. Plastic-embedded thin sections were imaged in a JEOL 1200 transmission electron microscope (JEOL), and digital micrographs recorded by means of an XR-100 CCD camera (AMT).

To prepare specimens for EPMA, frozen cultures were cryosectioned at −160 °C by means of a Leica Ultracut S/FCS cryoultramicrotome. Freeze-dried cryosections were imaged and analyzed in a Zeiss EM912 Omega analytical electron microscope (Carl Zeiss) using a ProScan 2K slow-scan CCD camera controlled by AnalySIS image processing software (Olympus Soft Imaging Solutions). X-ray spectra were recorded and processed by established procedures (3).

Chemicals and Reagents. Bicuculline, 6-cyano-7-nitroquinoxaline-2,3-dione (CNQX), 1-[2-(4-hydroxyphenoxy)ethyl]-4-[(4-methylphenyl)methyl]-4-piperidinol hydrochloride (Co 101244), ifenprodil, nimodipine, (±)-(*R**, *S**)-α-(4-hydroxyphenyl)-β-methyl-4-(phenylmethyl)-1-piperidinepropanol maleate (Ro 25–6981), picrotoxin were from Tocris Bioscience. NeuN antibodies were from Chemicon. All other reagents were purchased from Sigma-Aldrich.

1. Grynkiewicz G, Poenie M, Tsien RY (1985) A new generation of Ca2+ indicators with greatly improved fluorescence properties. *J Biol Chem* 260:3440–3450.
2. Nicholls DG (2006) Simultaneous monitoring of ionophore- and inhibitor-mediated plasma and mitochondrial membrane potential changes in cultured neurons. *J Biol Chem* 281:14864–14874.
3. Pivovarova NB, et al. (2004) Excitotoxic calcium overload in a subpopulation of mitochondria triggers delayed death in hippocampal neurons. *J Neurosci* 24:5611–5622.

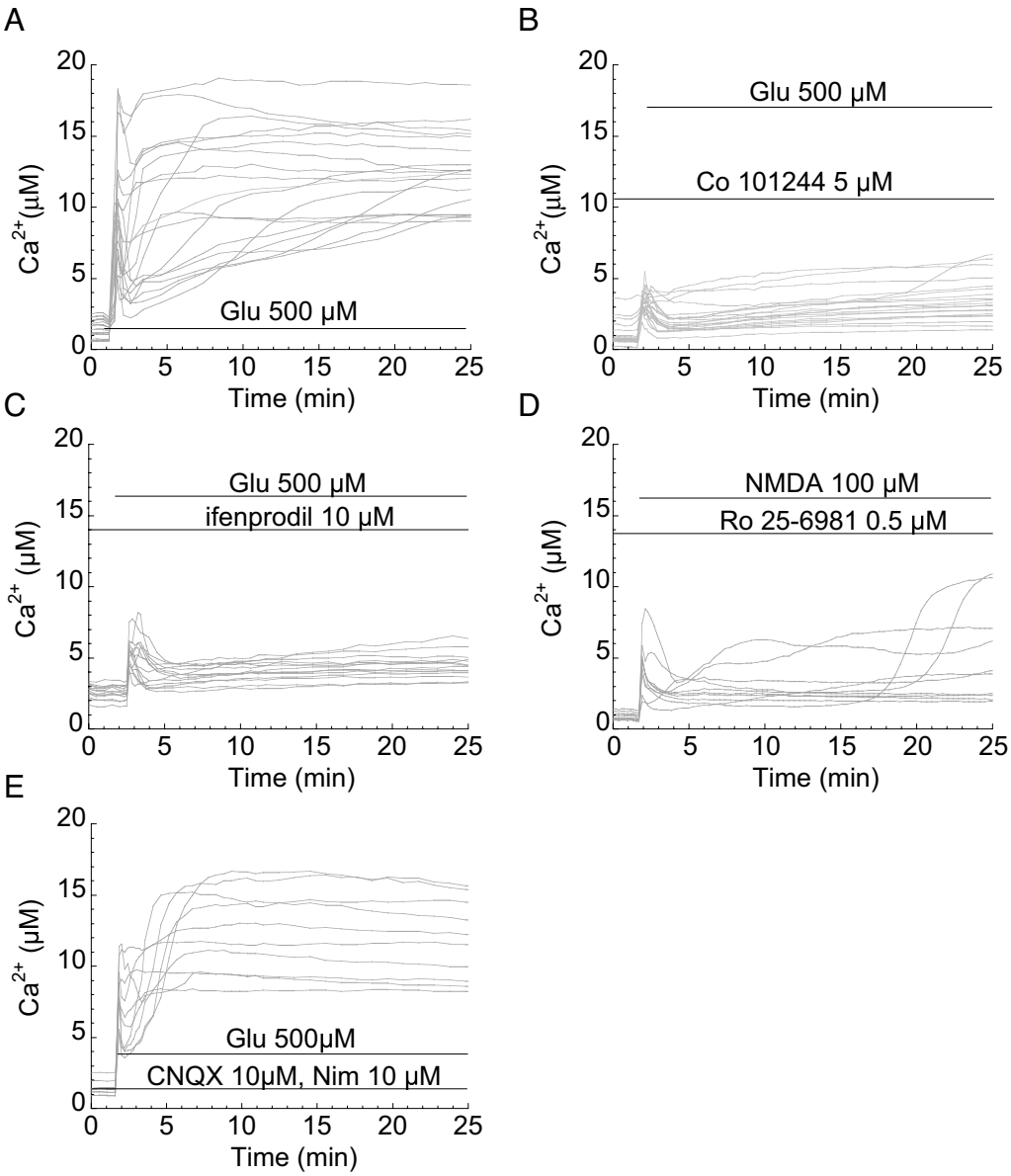

Fig. S1. Single-cell quantitative ratiometric traces of intracellular free Ca^{2+} concentration changes (fura-2FF, representative experiments) from young cells (14 DIV) exposed to glutamate alone (Glu) (*A*) or in the presence of Co 101244 (*B*), ifenprodil (*C*), or to NMDA in the presence of Ro 25–6981 (*D*). Excitotoxic Ca^{2+} elevations are strongly reduced by the NR2B antagonists in the majority of cells. CNQX plus nimodipine (*E*) had no effect on glutamate-evoked Ca^{2+} elevations.

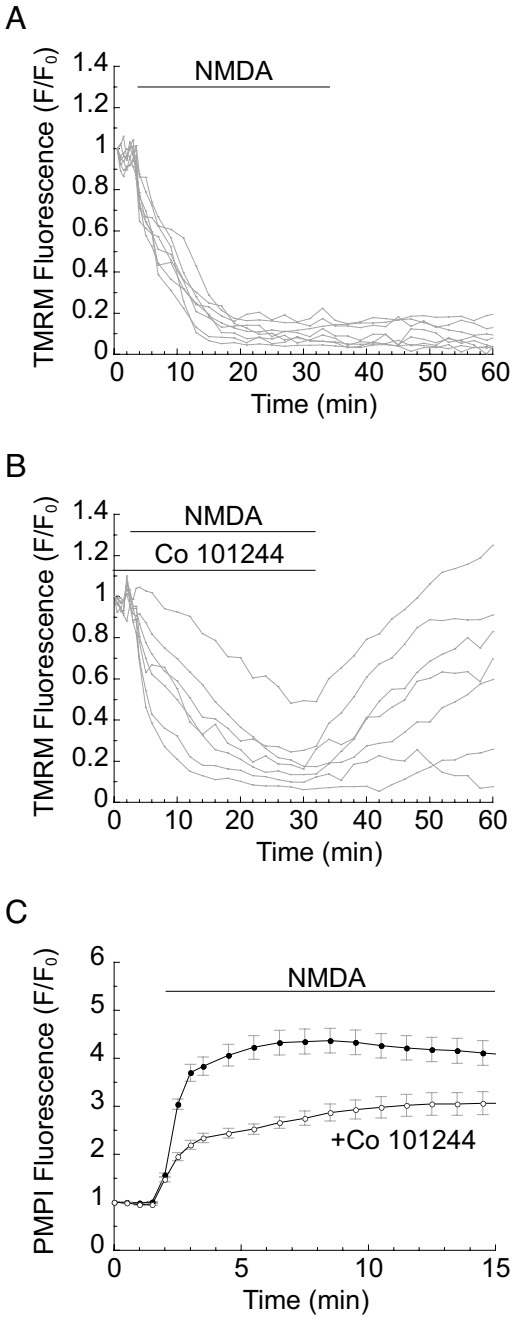

Fig. S2. NMDA-induced changes in TMRM and PMPI fluorescence are reduced by NR2B antagonist. (*A* and *B*) Single-cell TMRM fluorescence traces in the absence (*A*) or presence (*B*) of Co 101244. Inhibition of NR2B-containing NMDARs slightly slows and attenuates the otherwise fast and nearly complete loss of TMRM fluorescence induced by NMDA; drug washout leads to essentially full fluorescence recovery in 75% of cells. (*C*) NMDA induces strong plasma membrane depolarization, as indicated by the large increase in fluorescence of the plasma membrane-selective probe PMPI. Traces are averaged, normalized fluorescence ± SEM from cells exposed to NMDA (100 μM) in the presence ($n = 15$) or absence ($n = 16$) of the NR2B antagonist Co 101244 (5 μM). NR2B blockade attenuates but does not abolish NMDA-induced plasma membrane depolarization.

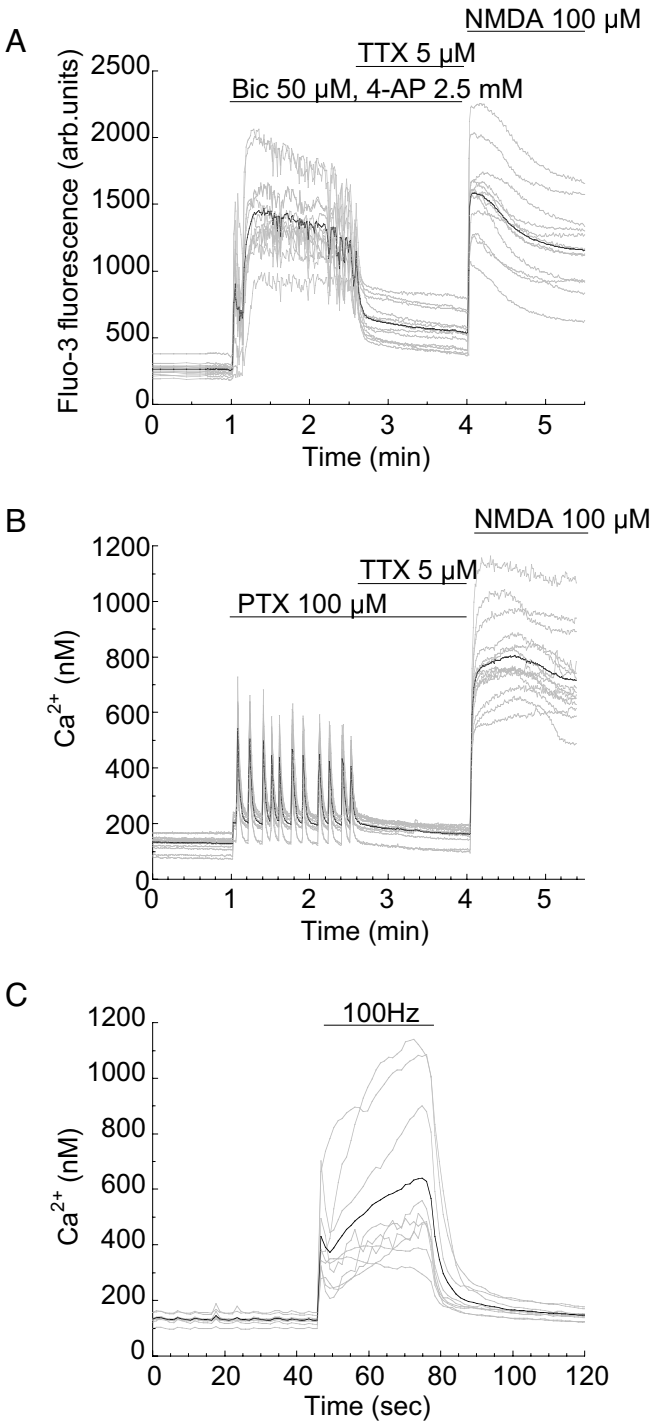

Fig. S3. Fluorescence traces revealing cytosolic free Ca^{2+} concentration changes after indicated treatments as reported by the high-affinity probes fluo-3 (*A*, $n = 12$) and fura-2 (*B*, $n = 14$; *C*, $n = 9$). Synaptically activated, TTX-sensitive Ca^{2+} elevations induced by exposure to bicuculline or picrotoxin, or by high-frequency field stimulation, appear to be comparable in amplitude to those induced by NMDA bath application, but this is misleading because both probes significantly underestimate the large NMDA-induced Ca^{2+} concentration increases (compare with Fig. 1*C* or Fig. 2*A*). Quantitative ratiometric records from fura-2 loaded cells show that synaptic activation by GABA inhibition (*B*) or field stimulation (*C*) induces Ca^{2+} spikes whose amplitudes are on the order of 500 nM. Black traces in all panels represent average responses.

Table S1. Effects of excitotoxic and synaptic stimulation on elemental concentrations in cytoplasm and mitochondria of cultured hippocampal neurons

	n	Na	Mg	Cl	P	K	Ca
Cytoplasm							
14–17 DIV							
Control	40	42 ± 7	51 ± 5	39 ± 5	557 ± 42	603 ± 29	0.6 ± 1.1
Glutamate	34	777 ± 53*	35 ± 6	529 ± 28*	397 ± 37	62 ± 13*	37 ± 3*
NMDA	48	731 ± 48*	31 ± 4	630 ± 50*	363 ± 40	51 ± 4*	47 ± 4*
NMDA + MK	30	16 ± 4**	40 ± 2	67 ± 7**	513 ± 18	555 ± 19**	3.2 ± 1.1**
NMDA + Co	45	519 ± 48**	51 ± 4	247 ± 21**	525 ± 27	142 ± 25**	4.3 ± 1.7**
NMDA + Ro	15	414 ± 60**	59 ± 9	250 ± 23**	599 ± 36	292 ± 32**	15 ± 5**
Bic	40	73 ± 14	40 ± 11	117 ± 21	618 ± 67	578 ± 77	13 ± 3*
21–28 DIV							
NMDA + Co	44	751 ± 41	32 ± 4	671 ± 37	234 ± 22	47 ± 5	51 ± 4[a]
NMDA + Zn^{2+}	30	569 ± 39**	22 ± 4	460 ± 44**	314 ± 24	46 ± 7	44 ± 4
NMDA + Co + Zn^{2+}	24	369 ± 10**	18 ± 2**	223 ± 11**	223 ± 13	89 ± 10**	6.5 ± 2**
Mitochondria							
14–17 DIV							
Control	45	15 ± 4	32 ± 2	21 ± 3	406 ± 12	368 ± 13	0.1 ± 0.8[b]
Glutamate	33	240 ± 27*	31 ± 4	175 ± 20*	820 ± 65*	55 ± 8*	910 ± 110*
NMDA	39	408 ± 60*	45 ± 10	302 ± 45*	938 ± 88*	34 ± 4*	1045 ± 123*
NMDA + MK	35	11 ± 3**	28 ± 2	33 ± 4**	377 ± 10**	314 ± 13**	0.6 ± 0.9**
NMDA + Co	52	245 ± 22	39 ± 3	125 ± 12**	443 ± 12**	144 ± 7**	8.5 ± 3.4**
NMDA + Ro	15	172 ± 34	39 ± 4	116 ± 21**	463 ± 25**	231 ± 22**	5.5 ± 4.5**
Bic	50	35 ± 3*	34 ± 4	87 ± 9*	488 ± 23	369 ± 22	6.7 ± 1.9
21–28 DIV							
NMDA + Co	26	446 ± 39	45 ± 6	417 ± 32	699 ± 42	30 ± 2	755 ± 73[a]
NMDA + Zn^{2+}	30	353 ± 64	41 ± 7	278 ± 51	654 ± 99	26 ± 5	656 ± 123
NMDA + Co + Zn^{2+}	15	99 ± 7**	63 ± 11	53 ± 6**	546 ± 54	101 ± 9**	359 ± 66**

Data are given as mean ± SEM in mmol/kg dry weight.

Cultures were frozen immediately after exposure to specified drug for 30 min. The number of neurons analyzed was 8–12 per each condition, taken from at least 2 different platings; *n* is the number of analyses.

Reagent concentrations were: bicuculline (Bic, 50 μM); Co 101244 (Co, 5 μM); glutamate (500 μM); MK-801 (MK, 20 μM); NMDA (100 μM); Ro 25–1969 (Ro, 0.5 μM).

*, ** Significantly different from control or from NMDA stimulation, respectively, at $P < 0.05$, by ANOVA with post hoc Dunnett multiple comparisons test for cytoplasm and by nonparametric Kruskal-Wallis rank ANOVA with post hoc Dunn's test for unbalanced data for mitochondria.

[a]Not significantly different from NMDA treatment.

[b]Below detection limit.